Ocean Engineering 299 (2024) 117424

Contents lists available at ScienceDirect

Ocean Engineering

journal homepage: www.elsevier.com/locate/oceaneng

Historical trends of floating wind turbine fatigue loads (Ireland 1920–2010)

Alain Ulazia [a,*], Hodei Ezpeleta [a], Gabriel Ibarra-Berastegi [b,c], Jon Sáenz [c,d], Nahia Martinez-Iturricastillo [e], John V. Ringwood [e]

[a] Energy Engineering Department, University of the Basque Country (UPV/EHU), Otaola 29, 20600, Eibar, Spain
[b] Energy Engineering Department, University of the Basque Country (UPV/EHU), Alda. Urkijo, 48013 Bilbao, Spain
[c] Plentziako Itsas Estazioa, University of the Basque Country (UPV/EHU), Areatza Hiribidea 47, 48620 Plentzia, Spain
[d] Department of Physics, University of the Basque Country (UPV/EHU), Sarriena Auzoa z/g, 48940 Leioa, Spain
[e] Centre for Ocean Energy Research, Maynooth University, Maynooth, Co. Kildare, Ireland

ARTICLE INFO

Keywords:
Offshore wind energy
Fatigue loads
Cluster analysis
ERA20C
ERA5
OpenFAST
Climate change

ABSTRACT

We present a new method for analysing the fatigue loads of offshore floating wind turbines over the long term. In this method, bias-corrected wind and wave data from the 20th century (ERA20C versus ERA5 reanalysis) is used for an energetic sea location in western Ireland. To reduce the computational cost and theoretical complexity, the sea states were clustered into categories to indicate how these categories evolve over three climate periods during a period of 30 years (1921–1950, 1951–1980, and 1981–2010). OpenFAST aeroelastic code simulation in floating mode was then conducted at each sea state for spar-type 5-MW and semi-submersible 15-MW wind turbines. This shows the damage loads and fatigue increments over the century, with some relevant cases (rotor torque, blade pitch and flapping, and tower side–side and fore–aft moments) showing fatigue increments of 5%–8%. Thus, in the new method, historical data are used to create a model to represent the evolution of sea states and corresponding fatigue over the long term, which can be applied globally to future projections.

1. Introduction

Renewable energy sources, as well as all other natural entities, are strongly affected by climate change as it constantly changes their constitutional characteristics. In the context of meteorological data and energy resources, the long-term effects of climate change are usually denoted as variations in the attributes of energy resource over periods of 30 years, also known as climate periods (Saenz-Aguirre et al., 2022). These periods of 30 years are those used by the World Meteorological Organization (WMO) to define climate norms (WMO, 2017), which are statistical values representative of a climatological element. In analyses related to the possible long-term variation of renewable energy resources, the usual approach involves the estimation of the constitutional characteristics of the resource in each climate period, calculation of the power density associated with these characteristics, and determination of their slow temporal variations as positive/negative changes per tri-decade (30 year period) (Pereira et al., 2013).

Considering the rapid industrial development in recent decades and continuous growth prospects (Jenniches et al., 2019), wind can be considered as the most significant renewable resource in the green energy generation infrastructure. The energy resource intensity term related to meteorological wind is the wind power density (WPD), whose temporal evolution (Carreno-Madinabeitia et al., 2021; Ulazia et al., 2023a) and geographical variability (Ulazia et al., 2019b) have widely been analysed in the literature, even considering the errors induced by the variations of air density, not only wind speed.

In recent years, the main focus of the wind power industry has been the promotion of the offshore sector. In this context, reviews of the policies and risks associated with offshore wind power have been conducted for different locations, such as the United Kingdom (Higgins and Foley, 2014) and China (Chen, 2011), showing its great potential. Thus, the design and development of wind turbines in offshore locations using both bottom-fixed and floating technologies have been analysed and gradually incorporated into the industrial manufacturing process of turbines (Guo et al., 2022). Far offshore locations with turbines that generate hydrogen but are not connected to the grid are also under techno-economic assessment (Babarit et al., 2018; Jang et al., 2022).

This expansion of offshore wind power technology is attributed to a stronger wind speed resource and reduction in restrictions and visual impacts at coastal/oceanic sites. Conversely, oceanic wave resources (and their evolution) in these offshore sites affect the performance

* Corresponding author.
E-mail addresses: alain.ulazia@ehu.eus (A. Ulazia), hezpeleta001@ikasle.ehu.eus (H. Ezpeleta), gabriel.ibarra@ehu.eus (G. Ibarra-Berastegi), jon.saenz@ehu.eus (J. Sáenz), nahia.martineziturricastillo.2023@mumail.ie (N. Martinez-Iturricastillo), john.ringwood@mu.ie (J.V. Ringwood).

https://doi.org/10.1016/j.oceaneng.2024.117424
Received 21 December 2023; Received in revised form 5 March 2024; Accepted 6 March 2024
Available online 11 March 2024

List of Abbreviations

AEP	Annual Energy Production
DEL	Damage Equivalent Load
DTU	Denmark Technical University
ECMWF	European Centre of Medium-Range Weather Forecasts
ERA5	ECMWF's 5th reanalysis
ERA20C	ECMWF's 20th century reanalysis
ERA20CC	Calibrated ERA20C versus ERA5 reanalysis
FAST	Fatigue, Aerodynamics, Structures and Turbulence
FWT	Floating Wind Turbine
IEA	International Energy Agency
LSS	Lower support structure
MARA	Maritime Area Regulatory Authority
NREL	National Renewable Energies Laboratory
ORESS	Offshore Renewable Electricity Support Scheme
PDF	Probability Density Function
QM	Quantile matching
QM_i	Quantile matching in the ith interval
SSP	Shared Socioeconomic Pathway
WEF	Wave Energy Flux
WMO	World Meteorological Organization
WPD	Wind Power Density
LSSGagMya	Rotating y-axis bending moment at the LSS [kN m]
LSSGagMza	Rotating z-axis bending moment at the LSS [kN m]
RootMxb1	Edgewise bending moment at the blade root [kN m]
RootMyb1	Flapwise bending moment at the blade root [kN m]
RootMzb1	Pitch bending moment at the blade root [kN m]
RotTorq	Rotor torque, constant along the LSS [kN m]
TwrBsMxt	Side–side bending moment at the tower base [kN m]
TwrBsMyt	Fore–aft bending moment at the tower base [kN m]
TwrBsMzt	Torsional bending moment at the tower base [kN m]

Nomenclature

H_s	Significant wave height
$H_s dir$	Incoming direction of waves (degrees clockwise from North)
L	Wavelength
m	Material exponent for fatigue calculation
P_c	Probability of occurrence of each cluster
T_p	Peak wave period
U_{10}	Wind speed at 10-m height
U_{z_H}	Wind speed at hub height
U_{dir}	Incoming direction of wind (degrees clockwise from North)
$U_{q05,i}, U_{q95,i}$	Wind speed centroid confidence interval at 95%
z_0	Roughness of the sea
z_H	Hub height

of wind turbines and must therefore be considered during the design process and validation analysis of their performance. Additionally, the development of wave energy converter (WEC) systems that has occurred in parallel in recent years (Jin et al., 2022) has also turned the focus of numerous analyses towards long-term analysis and climate change-related evolution of wave energy resources (Jin et al., 2022; Ulazia et al., 2023b), or the progress in combined wind and wave energy harvesting devices (Kalogeri et al., 2021).

Meteorological wind, oceanic waves, and their corresponding indices (WPD and wave energy flux (WEF)) have experienced variations owing to climate change since the pre-industrial era. In this context, the global reanalysis ERA20C (see Section 2.2) data are a unique source for this type of historical analysis and have indicated significant changes in wind and wave energy, mainly measured according to increments in wind speed and wave height under different climates, such as in Chile, Iceland, and the Iberian Peninsula (Ulazia et al., 2018; Penalba et al., 2020; Carreno-Madinabeitia et al., 2021).

Such variations in meteorological winds and oceanic waves owing to climate change will have a significant effect on the overall performance of offshore renewable energy generation systems as their performance depends on the characteristics of these natural resources. An example of an estimate of the annual energy production (AEP) based on wind-speed measurements and the use of a probability density function (PDF) is presented in Liang et al. (2022). An example of the discretization of the effects of a resource (oceanic waves) on the power production and fatigue mechanical load fatigue of floating turbines is presented in Saenz-Aguirre et al. (2022). Therefore, in general, the application of the estimated characteristics of the resource at specific climate periods to energy generation systems directly enables the measurement of the effects of each characteristic on their performance, and can help determine the interaction between climate change and the performance of energy generation systems.

In this study, the energy generation and mechanical load fatigue of different scaled floating wind turbines (FWTs) at specific offshore locations in Ireland were estimated and compared across different climate periods. The objective of this study was to identify the effect of past long-term climate change patterns on wind turbine energy generation and mechanical load fatigue using an associated quantitative numerical assessment. Although the proposed analysis provides a retrospective vision of the effect of climate change on the performance of floating turbines, the same analysis conducted with future meteorological resource projections could provide a prospective vision for predicting the future effects of mechanical fatigue on wind turbines at specific locations.

Ireland was the geographical location for our analysis and origin of the meteorological data. Ireland has garnered special interest in the development of offshore renewable energies considering that its maritime area is seven times larger than its landmass, with significant wave and wind resources. This vast expanse is primarily situated along the West Coast in the Atlantic Ocean (Maritime Area, 2023), where the waters are relatively deep but do not exceed 200 m on the continental shelf. Consequently, these waters offer an ideal environment for the deployment of floating structures for harnessing offshore renewable energy sources.

The newly constituted Maritime Area Regulatory Authority (MARA) is the state agency responsible for accelerating the development of offshore renewable energy in Ireland through the administration and management of the licencing and development of offshore renewable energy projects (Maritime Area, 2023). In May 2023, Ireland conducted its inaugural offshore wind farm auction, referred to as the Offshore Renewable Electricity Support Scheme (ORESS), wherein a combined capacity of nearly 3.1 GW was auctioned with 450 MW on the west coast (EirGrid Group, 2023), and the restructuring of the Galway port is planned to accomplish future offshore wind implementation, operation, and maintenance support. Subsequently, before mid-2024, a second auction, namely, ORESS 2.1, was scheduled to allocate an additional capacity of 900 MW (Government of Ireland, 2023).

The region west of Ireland is an interesting offshore area from the perspective of future global climatology and climate change. The collapse of the Atlantic Meridional Overturning Circulation (AMOC) in Ireland could potentially influence offshore wind and wave energy (Warning, 2023). Previous studies have provided information on wind and wave resources off the Irish coast, as well as the interaction between waves and wind (Fusco et al., 2010), indicating that Ireland has a high potential for wind and wave energy (Gaughan and Fitzgerald, 2020). Studies have shown that wind speeds range between 9.6 and 12.3 m/s at the typical hub height, making it suitable for wind energy development (Remmers et al., 2019). However, the variability and correlation between wind and wave resources differ depending on the location (Fusco et al., 2010). The shape of the wind profile and wind shear are important factors in determining the offshore wind turbine performance, and waves can influence these factors (Gallagher et al., 2016). A wave field can modify the wind field, thereby affecting the wind profile and turbulence levels (Kalvig et al., 2014). Additionally, the complementarity between wind and wave energy resources has been highlighted (Fusco et al., 2010), suggesting the potential for combined wind-wave energy installations. This information suggests that changes in ocean circulation patterns could potentially affect wind and wave resources and their interaction, which is a key issue considering the strong changes observed in previous studies on the long-term analysis around this Atlantic area related to wave height, wave period, and wave energy connections between the Bay of Biscay, west of Ireland, and Southern Iceland (Penalba et al., 2018; Ulazia et al., 2019a; Penalba et al., 2020; Ulazia et al., 2023b,a).

The estimated energy generation and mechanical load fatigue were computed using two different wind turbine models, both of which have significantly different rated powers and represent the evolution of the wind power industry over the last decade. On the one hand, the NREL 5 MW turbine (Jonkman et al., 2009) with an OC3-Hywind spar-type flotation system (Jonkman, 2010) is a representation of recent wind turbines and currently used technology. In contrast, the IEA-15 MW turbine (Gaertner et al., 2020) is an eagerly anticipated product considered to represent the current efforts of the industry. In both cases, the dynamics of the wind turbine were modelled using the open-source aeroelastic model OpenFAST v3.1.0 (OpenFAST, 2023), developed and supported by the National Renewable Energy Laboratory (NREL), which is a highly detailed simulation environment for both onshore and offshore wind turbines and has been widely used and accepted in the literature (Golparvar et al., 2021; Jonkman et al., 2021).

MLife *Matlab*-based tool (The MathWorks Inc., 2022) is integrated in OpenFAST for post-processing results from wind turbine simulations. The short-term fatigue calculations are based on input files and include short-term damage-equivalent loads (Damage Equivalent Loads or DELs) and damage rates. Similarly, the lifetime fatigue calculations are based on the entire set of input files, a design lifetime period, an availability factor, and a wind speed distribution, including lifetime DEL, lifetime damage, and time until failure (Hayman and Buhl, 2012).

Several authors have recently studied the relation between climate change and offshore wind turbine fatigue loads, showing a new perspective that not emphasizes only the affection of global warming on energy generation. They underline that, at least, similarly important is the effect on loads acting on wind turbines that can reduce their lifetime. In case of Hübler and Rolfes (2021), they also use OpenFAST simulations for 5 MW turbine with a probabilistic approach, but only a fixed mode, without considering the relevant effect of waves in the behaviour of floating systems. Wilkie and Galasso (2020) use NREL 5MW referential turbine combining wind and waves to show that fatigue damage is more sensitive to climate change effects than energy density, using surrogate models (also known as metamodels or emulators), which replace the expensive time–history simulations with intelligently chosen simulations, as in our clustering methodological approach. However, the offshore turbine is also monopile based, and they do not consider the floating system, as in the case of other authors James et al. (2023). To the best of our knowledge, this is the first study that relates historical climate change and FWT's integral fatigue evolution for various elements of the FWT, although particular damage assessments of important elements such as mooring systems has not been developed in this case (Du et al., 2020).

The remainder of the paper is structured as follows. The wind and wave meteorological resource data is described in Section 2.2. The wind turbine models and simulation environment used in the analysis are described in Section 2.3. In Section 2.4 a detailed explanation of the methodology is provided, followed by the characterization of the climatological normal period using cluster analysis and the calculation of the power production and mechanical fatigues of the FWT. Sections 3 and 4 present the results and discussion, respectively. Finally, conclusions and future outlook are presented in Section 5.

2. Data and methodology

A description of the study area is provided in Section 2.1. The historical meteorological data and offshore locations selected for analysis are presented in Section 2.2. The characteristics of the FWTs used in the analysis and simulation environments are described in Section 2.3. Finally, the methodology for assessing the energy generation of FWTs and the mechanical load fatigue of their main components is described in Section 2.4.

2.1. Study area

West Ireland around Galway Bay is one of the most energetic sea states in Europe, in terms of both the wind and wave energy (Gallagher et al., 2016; Penalba et al., 2018; Remmers et al., 2019). The Irish government plans to expand the port of Galway to undertake future operations and maintenance (O&M) work for FWTs and wave-energy farms in this area (EirGrid Group, 2023; Government of Ireland, 2023).

The bathymetry of the study area is shown in Fig. 1, indicating significant areas to the west of Ireland with bathymetry less than 1000 m for the possible anchoring of FWTs (Ulazia et al., 2016, 2017; Goncalves et al., 2017). The majority of this vast expanse lies at depths that do not exceed 200 m on the continental shelf (see the zoomed map below), constituting a special area for FWTs in Europe that unifies Ireland and UK (Maritime Area, 2023). The selected gridpoint at (10°W, 53°N) is also represented (red star).

As mentioned previously, the expected collapse of the AMOC during the following decades (Warning, 2023) can significantly affect the long-term conditions of offshore wind and wave energy in Ireland; therefore, it is essential to study past long-term behaviour as a referential precedent. The global databases to study these changes for wave and wind are described in the next section and Table 1, which are calibrated within the study area showed in Fig. 1.

2.2. Historical meteorological data

2.2.1. ERA20C

The ERA20C reanalysis is a climate reanalysis dataset covering the period of 1900–2010. It assimilates observations of surface pressure and surface marine winds from the historical International Comprehensive Ocean-Atmosphere Data (ICOADS) (Freeman et al., 2019). This was an outcome of the European Reanalysis of Global Climate Observations (ERA-CLIM) project. The ERA20C reanalysis provides a comprehensive and consistent description of the global atmosphere, including the temperature, pressure, wind, humidity, and precipitation (Poli et al., 2016). It is used by scientists and engineers in various fields, including climate research, weather forecasting, and wind and wave energy modelling (Bloomfield et al., 2018; Ulazia et al., 2018, 2019a; Wohland et al., 2019).

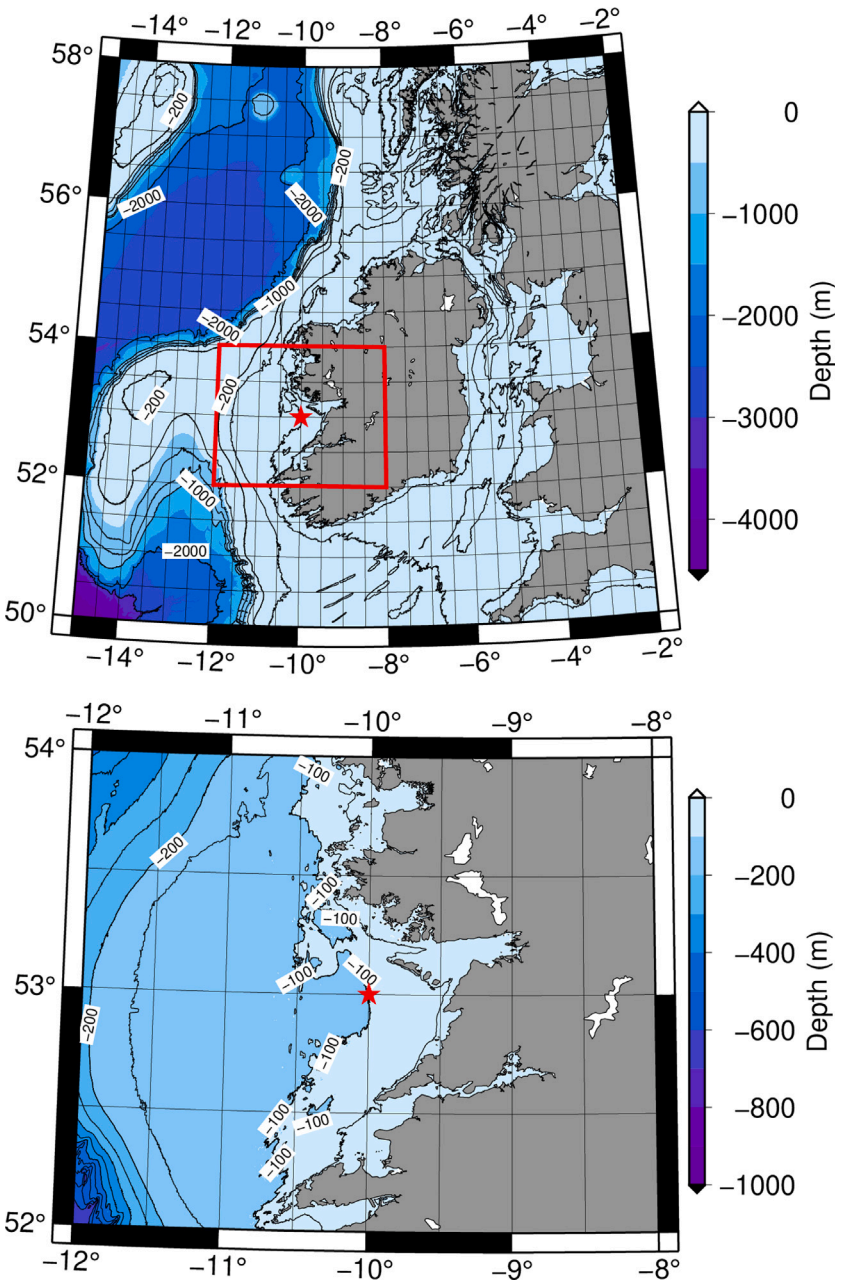

Fig. 1. Bathymetry around Ireland (above). Note the broad shallow bathymetric area on the west where FWTs can be installed at less than 1000 m depth. Panel below: detail of the bathymetry inside the red square marked in the figure on the left. Note the shallow waters around the study area. The selected gridpoint at (10°W, 53°N) is also represented (red star). Note that the spatial resolution of the grid is of 125 km.

2.2.2. ERA5

The ERA5 reanalysis data (Hersbach et al., 2020) from 1950 to 2020 were used as the calibration base (bias correction) against the corresponding intersection period of ERA20C to study the wind and wave conditions at a point near Galway. The data were downloaded from the Copernicus Climate Change Service Climate Data Store (https://cds.climate.copernicus.eu/) for wind and waves. ERA5 is a widely used and validated source for wind and wave energy assessment, with several examples in recent years (Hayes et al., 2021; Kardakaris et al., 2021).

In this study, we focused on four variables for both ERA20C and ERA5: wind speed at 10 m (U_{10}), wind speed at 100 m (U_{100}), peak wave period (T_p), and significant wave height (H_s). The incoming directions of wind $Udir$ and waves H_sdir were also incorporated into the analysis. Table 1 lists the main properties of the two reanalysis exercises of the European Centre of Medium-Range Weather Forecasts (ECMWF), including the covered period and spatial and temporal resolutions.

Table 1
Features of ERA20 and ERA5 according to their temporal and spatial resolutions.

Reanalysis	Period covered	Spatial	Temporal resolutions
ERA20	1900–2010	125 km	3 h
ERA5	1970–Present	30 km	1 h

2.2.3. Directional bias correction

Considering the importance of direction in this analysis and for FWTs, a directionally classified quantile-matching technique was used. Although this technique is referred to in the literature as probability mapping (Block et al., 2009), quantile mapping (Sun et al., 2011),

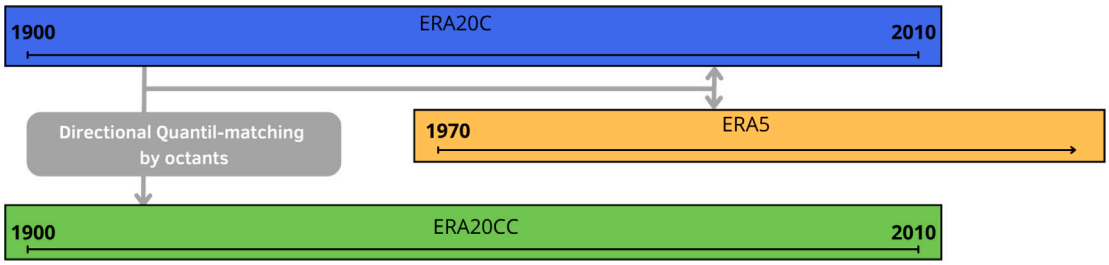

Fig. 2. The intersection period of ERA20C versus ERA5 is represented, in which the calibrated data of ERA20CC after directional bias correction is obtained.

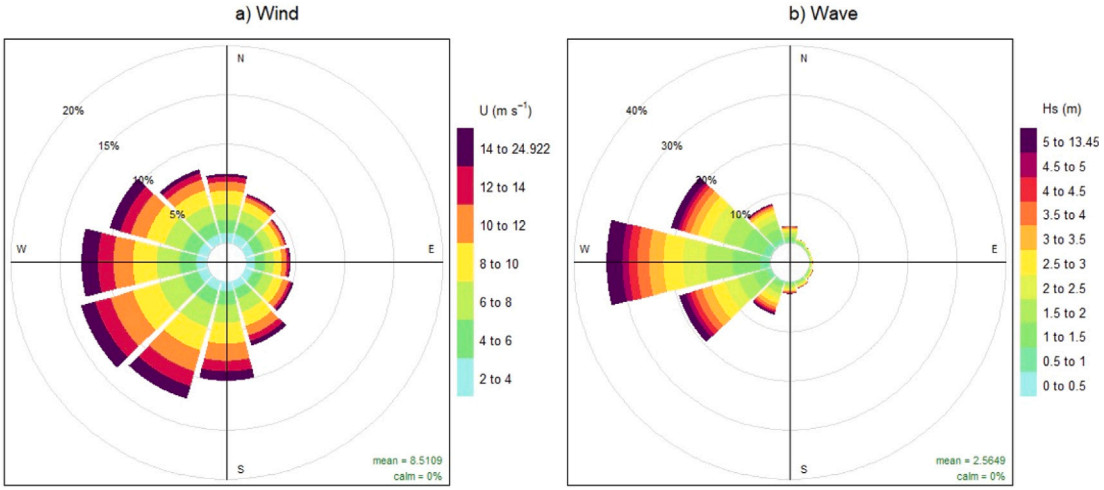

Fig. 3. (a) Wind and (b) wave rose diagrams at the selected location in the west of Galway Bay. 12 angular intervals are used in relation to each transference function for the bias correction, as defined in Eq. (1).

histogram equalization (Rojas et al., 2011), and statistical downscaling (Piani et al., 2010), the calibration or bias correction of a model is the process of adjusting the model output to match the observed data (Maraun, 2010; Teutschbein and Seibert, 2011; Vamsikrishna et al., 2012). This is typically conducted using the classified quantile matching (QM) method. In this case, instead of constructing a unique transfer function, the calibrated source (ERA20C) and calibration base (ERA5) are divided into different classes (see Fig. 2, representing the temporal sketch) to obtain the calibrated time-series data of ERA20CC.

In climatology, creating categories with different ranges of temperature and pressure or wind and wave directions is typical, and a separate transfer function is used to adjust the output for each value range. In this case, directional categorization was used with 12 intervals and an increment of 30°.

$$[-15^\circ + 30^\circ(i-1), -15^\circ + 30^\circ i) \quad i = 1, 2, \ldots, 12, \tag{1}$$

to obtain 12 QM_i transfer functions for each interval based on the bias correction. To the best of our knowledge, this approximation via directional calibration has only been developed for the marine environment in a single previous study on the potential of Chilean wave energy (Ulazia et al., 2018).

This procedure was applied to the calibration of directional magnitudes, zonal and meridional wind speeds, and zonal and meridional projections of significant wave heights. The corresponding wind and wave compass roses for the entire period are shown in Fig. 3. These figures clearly show that the predominant direction is western, representing the 10th and 11th intervals, and the corresponding QM_{10} and QM_{11} are the key calibration vectors defining the first interval QM_1 for the northern component sector.

2.2.4. Wind vertical profile

As the reference height of the wind data is 10 m, a logarithmic vertical profile should be applied to obtain the wind speed at the turbine hub height z_H according to Eq. (2) (Manwell et al., 2010), where z_0 indicates the roughness of the sea. Table 2 lists the hub heights of both turbines together with other important characteristics, namely, 90 and 150 m for the 5-MW and 15-MW turbines, respectively.

$$U_{z_H} = U_{10}\frac{\log(z_H/z_0)}{\log(10/z_0)} \quad [\mathrm{m/s}] \tag{2}$$

After obtaining the significant wave height and peak period, namely, H_s and T_p, respectively, Hsu's law (Eq. (3)) is applied to obtain the instantaneous sea roughness z_0 at each realization of the time series; therefore, the wind speeds at both hub heights (Hsu, 2003; Ulazia et al., 2016) can be obtained from H_s and wavelength L, which establishes an empirical improvement based on dimensional calculus and Charnock friction wind speed, and validated for several buoy data in the North Atlantic (Manwell et al., 2010).

$$z_0 = 1200 H_s \left(\frac{H_s}{\mathrm{L}}\right)^{4.5} \tag{3}$$

For deep-water approximation, the wavelength (Holthuijsen, 2010) can be estimated from the mean wave period (Eq. (4)) using the dispersion law:

$$L = \frac{g T_p^{\,2}}{2\pi} \tag{4}$$

2.2.5. Division into climate periods

After calibration, the data were divided into three climate periods (1921–1950, 1951–1980, and 1981–2010) with the original temporal resolution of ERA20CC of 3 h (time series of 87 600 cases for each period). The selection of this reference period of 30 years corresponds to the current guidelines of the WMO (2017) for the definition of climatological standards. This method is also used by major meteorological data providers, such as the Copernicus Climate Change Service, in their

Table 2
Main characteristics of the baseline NREL 5-MW wind turbine.

	Value		Unit
	IEA-15 MW	NREL-5 MW	
Rated power	15	5	MW
Rotor diameter	240	123	m
Hub height	150	90	m
Hub diameter	7.94	3	m
Cut-in, rated, cut-out wind speed	3, 10.59, 25	3, 11.4, 25	m/s
Cut-in rotor speed	5	6.9	rpm
Rated rotor speed	7.56	12.1	rpm

climatological analyses (Copernicus C3S, 2021). The main reason for this choice was to remove the contribution of interannual variations, such as North Atlantic Oscillation (NAOP) or El Niño/a, which can result in significant variability up to the decadal scale, to obtain a clean trend under the influence of climate change (Ghil and Allen, 2002).

2.3. Floating offshore wind turbine model

The characteristics of the wind turbines considered in the analysis and the simulation environment for the performance of the FWTs are described in detail in this section.

2.3.1. Characteristics of the turbines

In this study, two FWTs with different characteristics were considered to evaluate the effects of the temporal evolution of climate-period-scaled meteorological data at an Irish offshore location on the energy generation and mechanical load fatigue of the selected FWTs. A sketch of both FWTs considered for the analysis is shown in Fig. 4.

The NREL 5-MW turbine (Jonkman et al., 2009), with an OC3-Hywind spar-type floating system (Jonkman, 2010), is included as a representative of the current status of wind power technology as turbines with rated power around this value have already been installed (e.g. OC3-Hywind-based 6 MW turbines have already been installed in Hywind-Scotland wind farm https://www.equinor.com/energy/hywind-scotland, (accessed on 30 May 2023)). OpenFAST (2023) offers an open-source aeroelastic model of the turbine developed by the NREL and is widely used in many studies.

Conversely, the IEA 15-MW offshore reference wind turbine (Gaertner et al., 2020), developed in a collaboration between the NREL, Technical University of Denmark (DTU), and International Energy Agency (IEA), is incorporated into the analysis as representative of the immediate future trend in the wind power industry, wherein large-scale turbines are being designed and validated for offshore applications. The open-source aeroelastic model of this turbine is compatible with OpenFAST (2023). Notably, OpenFAST-based simulation and analysis using a semi-submersible platform proposed by the University of Maine (Allen et al., 2020) is also supported.

The scaling up of the turbines was translated into the design of mechanical components with significantly greater dimensions (a sense of this can be deduced from the approximation in Fig. 4) and different operational parameters of the turbines in relation to the rotational speed and power production. The main geometric and operational parameters of both FWTs are presented in Table 2.

The motivation for the fatigue load assessment for both systems is that although both turbines have been designed for offshore floating energy generation systems, their different dimensions and operational designs may cause a significant difference in their sensitivity to changes in environmental conditions in terms of the power production and mechanical loads fatigue. Regarding the IEA 15-MW machine, by possessing a substantially higher power production, the absolute values of aerodynamic forces and fatigue will be much higher, but in relative terms of damage equivalent loads the fatigue should be the same to have a service life of 20–25 years. Furthermore, it may be more stable in terms of withstanding the effect of waves, and not only due to the reduction in the natural frequency of the floating system.

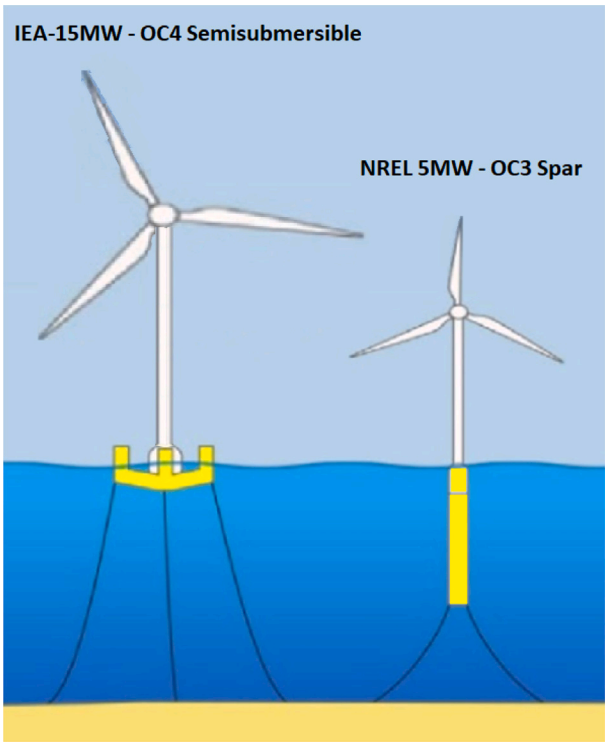

Fig. 4. Sketch of the floating turbines used in the analysis (Shafiee, 2023). (Notably, the dimensions are approximate and do not represent the real scale).

Table 3
List of bending moment elements selected for fatigue post-processing, named after their abbreviations in OpenFAST.

Name	Description	Unit
RootMxb1	Edgewise bending moment at the blade root	[kN m]
RootMyb1	Flapwise bending moment at the blade root	[kN m]
RootMzb1	Pitch bending moment at the blade root	[kN m]
RotTorq	Rotor torque, constant along the LSS	[kN m]
LSSGagMya	Rotating y-axis bending moment at the LSS strain gage	[kN m]
LSSGagMza	Rotating z-axis bending moment at the LSS strain gage	[kN m]
TwrBsMxt	Side–side (or roll) bending moment at the tower base	[kN m]
TwrBsMyt	Fore–aft (or pitch) bending moment at the tower base	[kN m]
TwrBsMzt	Torsional (or yaw) bending moment at the tower base	[kN m]

2.3.2. OpenFAST simulation environment

OpenFAST (2023) is an open-source simulation environment for diverse onshore/offshore wind-turbine configurations, including floating or bottom-fixed topologies. OpenFAST is an aeroelastic model that enables high-fidelity coupled dynamic evaluation of different wind turbines operating under various environmental conditions. OpenFAST includes multiphysics models, such as aerodynamics, hydrodynamics for offshore structures, control, and structural dynamics, and a user interface to define the environmental conditions of turbine operation.

Detailed mechanical modelling in OpenFAST enables the high-fidelity simulation of turbine behaviour, which can subsequently be used for performance or fatigue evaluation. OpenFAST has widely been used in the literature to analyse the behaviour of NREL 5-MW turbines for various purposes. It should be mentioned the effect of the control function on the behaviour of turbines (Lackner, 2009), or the design of different mechanical topologies and the resulting effects on structural loads (Li and Gao, 2015) can also be evaluated.

Table 3 lists the main bending moment elements for the fatigue analysis in this study, which were selected by considering their importance and relevance in evaluating long-term variation behaviour.

When simulating offshore turbines, the environmental conditions of both the wind and ocean can be defined to analyse the dynamic behaviour of the turbine under various conditions. The simulations were conducted with still air and turbulent wind speed. Waves can also be defined as regular or irregular with an adjustable peak period and significant height.

2.4. Methodology for energy generation and mechanical fatigue assessment

Fatigue damage for the tower and lower support structure (LSS) is calculated using material exponents m of 3, 4, and 5, while material exponents of 8, 10, and 12 are used for the blades. A low material exponent indicates a material that is ductile and easily deformed, while a high material exponent indicates a material that is brittle and resistant to deformation. These values were therefore chosen based on the material of each component: Steel for the tower and LSS, and composite for the blades (Haid et al., 2013), as shown in the tables of Section 3. Lifetime fatigue calculation is weighted by the probability distribution. However, short-term damage computation is not probabilistic, considering only the rainflow cycle counts from an individual time series (OpenFAST, 2023).

The methodology for estimating the generated energy and assessing the mechanical load fatigue was based on the methodology proposed in Saenz-Aguirre et al. (2022). According to this methodology, the following steps were followed:

- Meteorological data is clustered to get a reduced number of values to allow computational simulation feasibility.
- Each cluster's central value is simulated with the aeroelastic model OpenFAST, and considers 10 different NTM wind speed seeds (10 random realizations of the wind field) to reduce variability and increases robustness of the results, by minimizing the risk of reaching conclusions based on isolated events of 10 min according to IEC 61400-3 (Quarton et al., 2005). Turbulence intensity of category C is selected in OpenFAST, that is, a typical low turbulence for the ocean compared to onshore A and B categories. IEC establishes a relation between average wind speed and turbulence intensity for each category. Design load basis for offshore wind turbines establishes therefore this simulation period of 10 min with a standard time-step of 0.01 s for DLC11 and DLC12, normal state simulations, using JONSWAP or Pierson–Moskovitz wave distributions (Natarajan et al., 2016).
- To estimate energy generation, the average power production of the turbine at each cluster is calculated and converted into energy with the probability of occurrence associated with each cluster. The availability due to operation and maintenance issues is not considered.
- To assess mechanical load fatigue, the simulation results of the aeroelastic model are post-processed using the software tool MLife (Hayman and Buhl, 2012). Initially, standard Damage Equivalent Loads (DEL) are calculated which are later linked with the probability of occurrence of each cluster. This probability of occurrence is pondered by the Weibull parameters of the location and each 30y period, together with the confidence interval of each cluster, since they are pre-established parameters in the input files of the code.

A schematic overview of the flow of information for the calculation of the 30 year DEL is shown in Fig. 5.

For MLife post-processing, in order to consider sea state statistics, the fatigue DEL computation is generated using the probability of occurrence of each cluster wind speed P_U with its 95% confidence interval of its centroid (not shown in the tables for the sake of brevity), i.e. $U_z \epsilon\ [U_{z,q05}, U_{z,q95}]$ (Eq. (5)).

$$P_{U,i} = e^{-(\frac{U_{q05,i}}{c})^k} - e^{-(\frac{U_{q95,i}}{c})^k} \quad (5)$$

where N refers to the total number of clusters and $i \epsilon \{1, \ldots, N\}$.

Firstly, OpenFAST's standard Weibull scale and form parameters (c, k) are used to compute directly standard probability of occurrence $P_{U,i}$ for each range of the confidence interval in Eq. (5), where Weibull cumulative distribution is implemented within the corresponding i interval. Then, each cluster's statistical weight is provided by its probability of occurrence P_c of Table 4. Thus, MLife original fatigue DEL values are corrected with the ratio P_c/P_{st}, which already considers the statistical distribution of clusters' every parameter. The pondered value is the final DEL_f (see Eq. (6)).

$$DEL_f = \sum_{i=1}^{N} DEL_i \frac{P_{c,i}}{P_{st,i}} \quad (6)$$

Furthermore, new features have been added to this initial methodology of Saenz-Aguirre et al. (2022); specifically, handling of the wind direction has been adapted to the situation of already knowing it. The usual approach during the design process for wind turbines (when the design is done for the 20–30 years lifetime of the turbine in advance) is to consider wind aligned with the longitudinal axis of the floating platform and tower, which would result in the worst-case scenario for the tower fore–aft bending moment, since a worst-case scenario ensures lower load values in real situations. However, in this case, by knowing the wind direction, aeroelastic simulation has been carried out so that rotor is aligned to the wind, but wind is not aligned with the platform fixed longitudinal axis (North direction or 0°, x axis). As a result, fore–aft and side–side bending moments (moment around x and y axis) of the tower are more alike and closer to real behaviour, in which the wind direction is changing and is not always aligned with tower longitudinal axis.

In this study, the effect of climate data evolution on the mechanical load fatigue of FWTs was quantified rather than the comparison of fatigue with and without waves. The first climate period is used as a reference, and the relative mechanical load fatigue evolution is calculated with respect to this first period in the second and third 30-year climate periods of ERA20CC (see Sections 2.2.3 and 2.2.5).

3. Results

The results of the historical meteorological data analysis are presented in Section 3.1. The results of the cluster analysis are presented in Section 3.2. Finally, Section 3.4 presents the results relative to the calculation of fatigue mechanical load fatigue and their evolution during the analysed climate periods.

3.1. Met-ocean historical trend maps

Fig. 6 shows the spatial evolution of the wind (wind speed) and wave resources (H_s and T_p) over three tri-decades. The increment of the most energetic areas in the west with higher wind speeds, wave heights, and wave periods is clearly indicated, mainly in the step from 1921–1950 to 1951–1980, wherein the acceleration of global warming from the pre-industrial era was more pronounced. Table 4 shows the numerical values of this increment at the selected gridpoint after the cluster analysis.

The results of the cluster analysis and the corresponding fatigue estimation were obtained at the selected grid-point near Galway Bay at (10°W, 53°N) (see the black star symbol in Fig. 6).

3.2. Identification of cluster classes

To ensure the feasibility of the computational simulation of the one-hourly observations during the three periods, they were grouped into a reduced number of clusters. The evolution of the analysis until convergence is observed in the eight cluster aggrupations is shown in Fig. 7 at the selected point. The clusters represent combined wind-sea

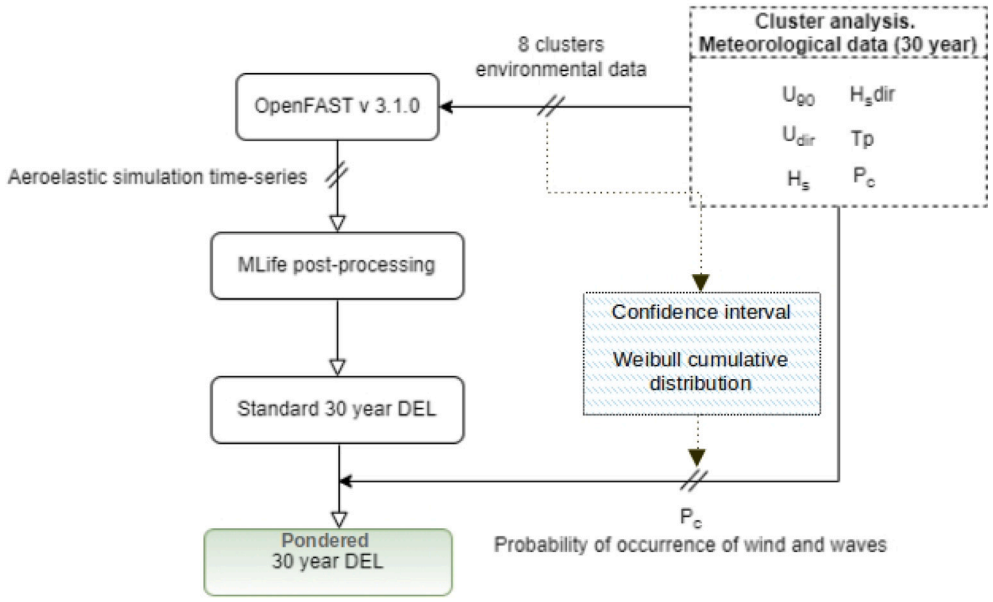

Fig. 5. Schematic diagram of the procedure for the estimation of the fatigue mechanical damage of the FWT.

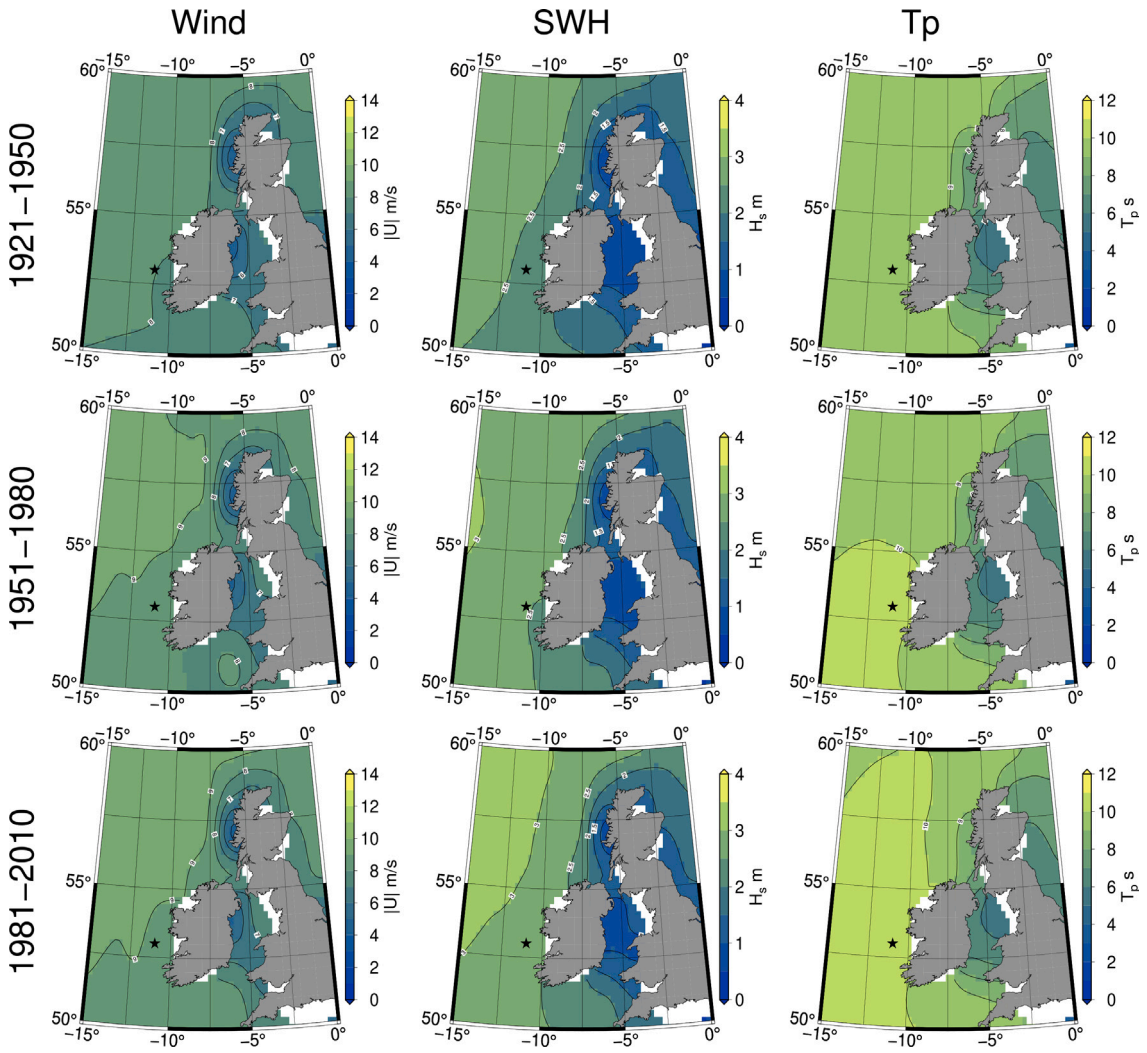

Fig. 6. Evolution of wind speed, significant wave height, and peak period during the three tri-decades. A black star symbol indicates the selected study point near Galway Bay at (10°W, 53°N).

Table 4
Clusters and percentage of occurrence. 10 OpenFAST simulations using a turbulent seed at category C (low turbulence) are performed for each cluster and each 30y period.

Cluster #	Period	U_{z_H} [m/s]	U_{dir} [°]	H_s [m]	$H_s dir$ [°]	T_p [s]	P_c [% of occurrence]
1	1921–1950	10.54	203.64	3.07	238.07	10.70	12.17
	1951–1980	10.74	203.00	3.14	237.41	10.80	14.06
	1981–2010	11.03	204.60	3.26	238.28	10.79	15.04
2	1921–1950	11.26	257.36	4.41	270.18	12.43	9.34
	1951–1980	11.56	259.28	4.59	271.71	12.52	11.54
	1981–2010	11.91	258.61	4.79	270.67	12.62	13.71
3	1921–1950	9.75	143.61	2.08	190.48	8.89	7.76
	1951–1980	10.09	143.70	2.25	189.74	9.22	7.86
	1981–2010	9.94	143.68	2.19	190.43	9.12	7.04
4	1921–1950	5.15	143.60	1.78	269.31	11.09	16.73
	1951–1980	5.38	133.78	1.87	271.86	11.26	17.73
	1981–2010	5.26	136.62	1.84	271.21	11.15	16.89
5	1921–1950	8.43	285.31	2.80	291.38	10.81	12.70
	1951–1980	8.62	285.43	2.95	294.95	10.98	14.45
	1981–2010	8.67	286.93	2.91	293.42	10.92	14.38
6	1921–1950	6.30	232.65	1.39	263.62	7.76	20.76
	1951–1980	6.53	233.11	1.47	264.53	7.93	15.34
	1981–2010	6.56	235.02	1.51	262.55	8.06	14.19
7	1921–1950	6.73	192.62	1.49	285.39	8.09	16.89
	1951–1980	6.99	185.54	1.61	288.88	8.36	16.28
	1981–2010	7.22	180.67	1.65	285.18	8.41	15.93
8	1921–1950	10.15	95.15	1.82	100.38	6.37	3.66
	1951–1980	10.89	93.20	2.10	98.81	6.78	2.74
	1981–2010	10.71	91.77	2.02	97.10	6.73	2.82

state types in the area obtained from data corresponding to the period of 1921–1950.

In this paper, Ward's algorithm has been used to group all cases into clusters (Murtagh and Legendre, 2014). Since the five wind and wave variables used (Table 4) have different units and ranges, at a initial stage, variables have been standardized to average 0 and standard deviation = 1. Then, each case is defined in the 5D hyperspace defined by those standardized five variables and the Euclidean distance is used to detect nearness (similarity). Following an iterative process, cases are grouped into clusters by the Ward's algorithm. Initially, each case is one cluster (Fig. 7) and as the calculations progress, similar cases are clustered together.

Furthermore, cases corresponding to the other two periods, namely, 1951–1980 and 1981–2010, were classified as belonging to one of the eight clusters or wind-sea state types. This classification was conducted by calculating the Euclidean distance to the cluster centroids and assigning each case to the nearest centroid. Throughout the entire period, the average distances to the clusters remained constant, indicating the stability of the wind-sea state types identified during the initial period.

The met-ocean data values corresponding to each cluster and each of the analysed climate periods are presented in Table 4. The information is presented in Table 4 for each cluster.

- Period [–] Climate period.
- U_{z_H} [m] Wind speed at hub height.
- U_{dir} [°] Incoming direction of wind.
- H_s [m] Significant wave height.
- $H_s dir$ [°] Incoming direction of waves.
- T_p [s] Peak wave period.
- P_c Frequency of occurrence of each cluster

Table 4 presents the eight wind-sea state types (centroids) derived from the observations during 1921–1950. Notably, for each type, in lines 1951–1980 and 1981–2010 (col #2), the average values of the wind and wave variables correspond to those two periods. Clusters #1 and #2 represent highly energetic wind-sea state types, and their frequency of occurrence has increased since the initial period of 1921–1950. In contrast, clusters #4, #6, and #7 correspond to poorly

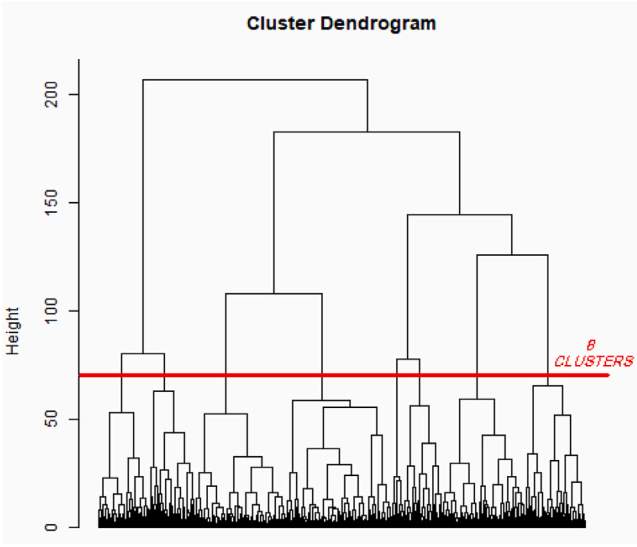

Fig. 7. Identification of clusters. Agglomeration tree obtained after the execution of Ward's algorithm for the first climate period (1921–1950).

energetic situations. Their frequency of occurrence have decreased or remained constant from the initial period. Finally, clusters #5 and #8 represent intermediate situations. These combinations of trends have contributed to an overall increase in energy from wind and wave variables since the initial period of 1921–1950 in the study area.

3.3. Energy generation

In this section, the power production is analysed at the selected location, and the mean power production is defined as the ratio of the total energy production to the hours contained in one climate period; and this is related to the wind speed in the power curve that indicates this power (equivalent wind speed).

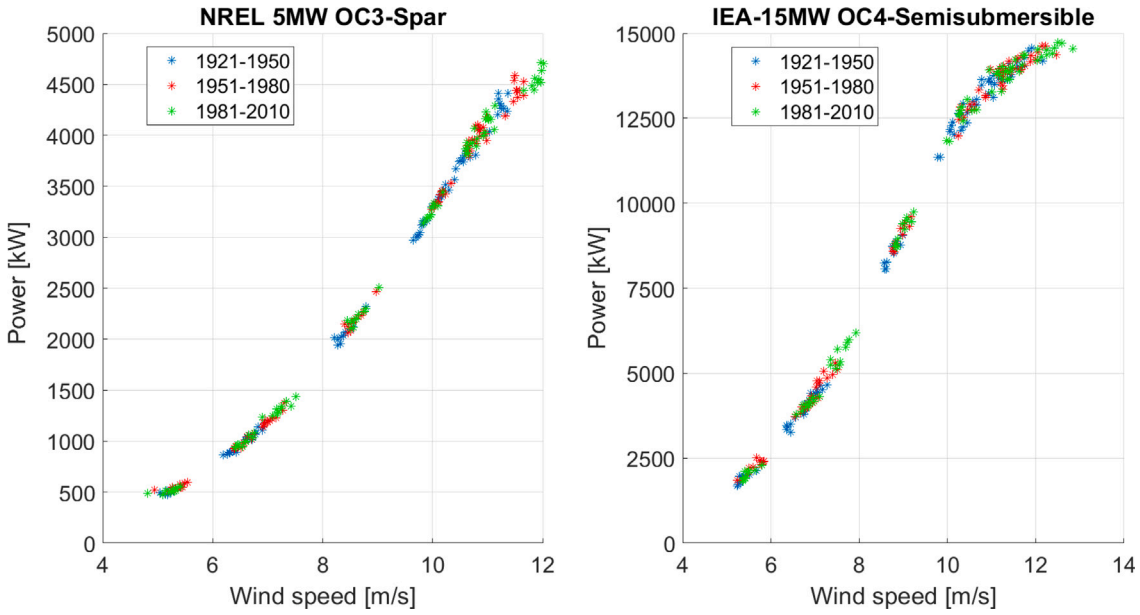

Fig. 8. Mean power productions for each period.

Table 5
Equivalent 30-year mean wind speed and energy generation [GWh] for each period.

	NREL 5 MW OC3-Spar		IEA-15 MW OC4-Semisubmersible	
	Eq. wind speed [m/s]	Energy [GWh]	Eq. wind speed [m/s]	Energy [GWh]
1921–1950	7.86	5087	8.16	19 127
1951–1980	8.27	5793	8.61	21 289
1981–2010	8.49	6159	8.86	22 316

Fig. 8 shows each climate period in three different colours on the power curves of both the 5- and 15-MW wind turbines. Fig. 8 qualitatively shows that the last climate period (green) presents wider ranges for more powerful cases (higher wind speed values) on the power curve, which is also related to the intervals of the cluster analysis. Note that this should be understood as a equivalent wind speed, constant wind speed that would generate the same energy, with the corresponding Weibull distribution that extends to the entire power curve.

Using the power values above in Fig. 8 corresponding to the centroid wind speed value of the cluster, and the probability value for each cluster, the energy generated during each 30 year period, in GWh, is estimated and shown in Table 5. That is, the power value $P(U_{z,c})$ (kW) of the power curve has been weighted by the probability P_c during the hours of the tri-decade.

$$Energy[GWh] = \sum_{Cluster} P(U_{z,c})P_c \cdot 365 \cdot 24 \cdot 30 \cdot 10^{-6} \quad (7)$$

This shows clear increments in the equivalent wind speed and energy production for both the second and third periods with respect to the pre-industrial era represented by the first climate period (i.e. 1921–1950). In relative terms, the increments are approximately 13–21 and 11%–16% for the 5-MW OC3-Spar turbine and 15-MW OC4-semi-submersible, respectively.

3.4. Assessment of the mechanical load fatigue

First, the absolute mechanical load fatigue used as a reference value is shown, followed by relative increments at the selected location. Therefore, all the results are structured for the three tri-decades and the two selected 5- and 15-MW turbines, which can be simulated using OpenFAST.

Table 6
30-year equivalent fatigue mechanical DELs ([kN m]) during 1921–1950 for the NREL 5-MW turbine and material exponents 3, 4, 5, 8, 10, 12.

	30 year fatigue DELs [kN m] for NREL 5-MW turbine					
	3	4	5	8	10	12
RootMxb1				11 936	12 558	13 006
RootMyb1				5772	6657	7385
RootMzb1				137	148	158
RotTorq	460	697	919			
LSSGagMya	5878	7032	7887			
LSSGagMza	5874	7030	7884			
TwrBsMxt	28 864	36 462	43 132			
TwrBsMyt	16 225	21 147	25 860			
TwrBsMzt	2548	2956	3366			

3.4.1. Reference absolute fatigue calculation

In this section, the reference values of fatigue mechanical DELs are presented. These values provide a reference point for the posterior relative increment calculation and analysis of the effects of the evolution of climatic properties on turbine mechanical load fatigue.

The reference absolute fatigue values for the NREL 5-MW turbine (in kN m) for the first three decades are listed in Table 6. Thus, an approximate validation was presented for comparison with typical fatigue results in OpenFAST reports for similar floating structures and turbines (OpenFAST, 2023; Jonkman et al., 2009; Jonkman and Matha, 2010).

The reference values of fatigue for the IEA 15-MW turbine (in kN m) during the reference period of the first tri-decade are presented in Table 7. Notably, this mainly serves as a comparative validation of typical reports using NREL's OpenFAST simulations (OpenFAST, 2023; Allen et al., 2020).

Table 7
30-year equivalent fatigue mechanical DELs ([kN m]) during 1921–1950 for the IEA 15-MW turbine and material exponents 3, 4, 5, 8, 10, 12.

	30 year fatigue DELs [kN m] for IEA 15-MW turbine					
	3	4	5	8	10	12
RootMxb1				58 471	62 038	64 513
RootMyb1				31 454	36 311	40 287
RootMzb1				608	652	687
RotTorq	1987	3098	4123			
LSSGagMya	17 946	22 156	25 602			
LSSGagMza	17 864	22 089	25 528			
TwrBsMxt	93 960	122 927	149 141			
TwrBsMyt	74 822	100 465	124 704			
TwrBsMzt	14 110	17 106	19 927			

3.4.2. Relative fatigue load evolution

The relative percentages of the fatigue load increments are listed in Tables 8 and 9 for both turbines and the two final tri-decades versus the first one. The fatigue load increments in the tower, shaft, and blades of the NREL 5-MW turbine are listed in Table 8. Different red colour gradients are used to rank the importance of these changes. Each case shows an increment from the second tri-decade to the final tri-decade, but the difference between the third and second tri-decade is less than that between the reference first tri-decade **RootMyb1**. This indicates that the flapping bending of the blade is the most affected fatigue parameter, and that the pitch bending **RootMzb1** is also significant. The rotor torque **RotTorq** is also significantly affected, although the gauge strain fatigue is irrelevant. According to the tower bending degrees of freedom, all three components are affected, with x and y components showing the strongest increment, namely, the side–side and fore–aft bending moments.

The stronger increment from first to second tridecade than from second to third one is a recurrent result in the historical analysis of climate change (mainly for wave and wind energy flux), where the effects of industrialization began to be noticed in the 60s and 70s of the past century, as the authors shows in their recent publications (Ulazia et al., 2018; Penalba et al., 2020; Carreno-Madinabeitia et al., 2021). However, future trends for wind and wave according to CMIP6 models show insignificant changes in the North Atlantic until 2100, showing even a small reduction in the West of Ireland Ibarra-Berastegui et al. (2023)

The relative fatigue load increments (in %) for the tower, shaft, and blades in the IEA 15-MW turbine are listed in Table 9. Red gradients were used to visualize different qualitative increments. Notably, an increment from the second tri-decade to the final tri-decade is indicated, but the difference is higher compared with that between the reference period. For blades, flapping bending is the most relevant type, along with pitch bending. The rotor torque was also significantly affected, but the effect was less than that of the 5-MW turbine. The gauge-strain fatigue increments were irrelevant for both the turbines. For the tower, the three components were also affected by higher values for the side–side and fore–aft bending moments. Therefore, the increment patterns are similar for both the 5- and 15-MW turbines.

Given these results, another important conclusion is that generally the increments shown in Tables 8 and 9 are almost independent to the material exponent for all the turbine elements. However, here is an exception in rotor torque for the last tri-decade: increment is 8.1% for material exponent 3, and 6.7% for material exponent 5.

4. Discussion

We proposed a new methodology for estimating the mechanical load fatigue of offshore FWTs over long periods by considering the estimated changes in wind and wave parameters. We used cluster analysis to identify the major wind-sea state types during a reference period and then analysed the evolution in their frequency of occurrence. By associating the fatigue damage with each cluster, we derived the fatigue trends over a 90-year period. This methodology reduces the computational cost and simplifies the estimation process, even though FWTs are more complex than onshore wind turbines owing to the additional impact of environmental variables of wave height, period, and direction, or offshore fixed monopile structures (Wilkie and Galasso, 2020; Hübler and Rolfes, 2021). As far as our knowledge, this is a pioneering attempt to analyse the relation between historical climate change and fatigue loads of floating turbines, with a novel directional calibration method and statistical bridge to connect long-term time series: wind and wave reanalysis data with rapid simulations of 10 min as paradigmatic cases given by clustering of sea states.

The authors have used clustering methods for wind energy in FWTs (Saenz-Aguirre et al., 2022) and wave energy (Ibarra-Berastegi et al., 2021; Carreno-Madinabeitia et al., 2024) to classify sea states and compute energy and fatigue production according to this typical values and its evolution. Here, it is demonstrated that 5–10 clusters are enough to have a metocean representation of almost 100% of the cases. The robustness and limitations of wind-wave climate clustering are well studied, and they are considered the best approximation to compute historical and future trends (Morim et al., 2019). In this sense, our metocean approximation with clusters simplifies the computation and the physical meaning of the DEL evolution, analysing the variation of centroids. We accept that this is a simplified approximation with limitations with respect to non-linearities and resonance effects on FWTs, but we think clustering is the best way to study long-term DEL evolution based on the variation in value and probability of main sea states through decades.

The increment patterns during the 20th century for both FWTs were similar for turbines with different nominal powers (5 and 15 MW) and floating platforms (spar-type and semi-submersible). However, the fatigue increments of the spar-type turbine were stronger for blades and towers, mainly for the rotor torque, with an increment of greater than 8% in the case of one material. Notably, the 5-MW spar-type turbine showed double the fatigue increment in the last tri-decade compared with the 15-MW semi-submersible in some cases such as rotor fatigue and material exponent 3 (see Tables 8 and 9). This involves a lifespan reduction of 8% for the rotor component of wind turbines, namely, from a typical lifespan of 20 years to almost 18 years. Through the techno-economic discussion, we determined whether the fatigue losses can be compensated for by the energy production increments presented in Table 5 for each turbine. One of the substantial aspect of this study is therefore the analysis of several important parts and elements of the FWT, but a key limitation should be emphasized related to lack of analysis on damage of the mooring system, a fundamental part of FWTs (Du et al., 2020).

By definition, with x the direction of wave incidence, fore–aft y and side–side x moments are the most affected for the tower, with small variations in z component fatigue related to yawing. In this aspect, this study has overcome the limitations related to the wind direction for a fixed longitudinal axis of the tower-platform system, getting similar bending values around x and y due to the change of direction angle in the simulations. The importance of full-direction wind flow for fatigue analysis has recently been underlined for other authors, because the non-Gaussian wind field strongly affects crack initiation life (Li et al., 2023). Furthermore, this directional analysis shows another counterpart for wake effect and yaw misalignment, which are also important for fatigue damage of floating turbines (Tao et al., 2023).

In the case of the blades, the increment in pitch fatigue is very relevant, a result that should be considered in relation to control design, and the flapping fatigue is also significantly affected over the decades, due to the deviation of the blades behind the rotor plane. However, the edgewise fatigue time variation is not significant, for both turbines.

The discussion of the increment results due to long-term climate change seems generally almost independent to the materials used in the tower, axis and blades. However, the rotor torque shows significant

Table 8
Relative increment (in [%]) of the fatigue mechanical DELs in 1921–1950 and 1981–2010 versus those in the reference tri-decade for the NREL 5-MW turbine.

	5 MW relative fatigue DELs vs. 1921–1950 [%]											
	1951–1980						1981–2010					
	3	4	5	8	10	12	3	4	5	8	10	12
RootMxb1				0.4	0.3	0.4				0.5	0.5	0.4
RootMyb1				7.7	8.6	9.1				9	9.8	10.2
RootMzb1				5.2	5	4.9				5.4	5.3	5.3
RotTorq	6.9	6.1	5.8				8.1	7.1	6.7			
LSSGagMya	1.7	1.5	1.5				1.6	1.4	1.4			
LSSGagMza	1.6	1.4	1.3				1.5	1.2	1.3			
TwrBsMxt	4	4.3	4.6				5.6	6	6.2			
TwrBsMyt	3.7	3.8	3.8				5.1	5.3	5.4			
TwrBsMzt	3.6	3.6	3.6				3.8	3.8	3.7			

Table 9
Relative increment (in [%]) of the fatigue mechanical DELs in 1951–1980 and 1981–2010 versus those in 1921–1950 for the IEA 15-MW turbine.

	15 MW relative fatigue DELs vs. 1921–1950 [%]											
	1951–1980						1981–2010					
	3	4	5	8	10	12	3	4	5	8	10	12
RootMxb1				0.2	0	0.2				0.1	0	0.1
RootMyb1				6.9	7.1	6.9				8.7	8.8	8.9
RootMzb1				3.8	4.1	4.2				4.5	4.9	5.1
RotTorq	3.4	3.6	3.6				4.5	4.6	4.7			
LSSGagMya	1.6	1.5	1.5				3.1	3.1	3			
LSSGagMza	1.5	1.5	1.5				3.1	3	3			
TwrBsMxt	4.9	5.4	5.6				6.4	6.6	6.5			
TwrBsMyt	3.7	3.9	4.1				5.3	5.4	5.6			
TwrBsMzt	1.9	1.6	1.1				2.6	2.5	2.6			

differences from material exponent 3 to 5 for the small turbine of 5 MW. The interpretation of this particular result from the viewpoint of materials is out of the scope of this article, but this should be underlined for mechanical engineers.

The most important application of the fatigue computation methodology over decades and for different sea states is related to future projections. Therefore, this study is a paradigmatic example of establishing and describing a novel method using historical data starting from the pre-industrial era, which constitutes the usual reference point for evaluating the effects of climate change. The use of deterministic time series corrected by the bias calibration of ERA20CC provides robustness to the results and corresponding conclusions, as well as the selection of a paradigmatic location to the west of Ireland, owing to its special climatic characteristics for wind and waves (Remmers et al., 2019; EirGrid Group, 2023; Government of Ireland, 2023).

Having established the methodology, in the future, this method can be applied globally at any interesting location using data from the last coordinated experiment of CMIP6, including physical downscaling models capable of simulating wave conditions (wave height and period) through atmospheric–ocean coupling models using CMIP6-derived input wind data (Eyring et al., 2016; Omrani et al., 2020; Nguyen et al., 2021).

5. Conclusions

We presented a novel methodology for the long-term analysis of fatigue loads for different offshore floating wind turbines using calibrated data (ERA20C versus ERA5 reanalysis) from the 20th century at an energetic sea location, namely, west of Ireland. This novel calibration technique creates directional bias-correction functions based on the invariance of cumulative density function, reinforcing the contribution of swell waves from the predominant direction.

The computational cost were reduced through the cluster categorization of sea states, which indicated the corresponding long-term evolution during climate periods of 30 years. Simulation in floating mode was then conducted under each sea state for spar-type and semi-submersible wind turbines of 5 MW and 15 MW, comparing turbines of different sizes and floating structures. The damage loads and fatigue increments during the tri-decades were 5%–8% in some relevant cases: rotor torque, blade pitch and flapping, and tower side–side and fore–aft moments. Both turbines show similar historical relative increments for same materials, but there are strong differences in the increments of rotor torque, which, paradoxically, is much higher for the small spar-type turbine.

The possibility of the space–time generalization of this methodology addresses a very relevant problem for future projections of fatigue in marine environments for floating wind turbines. Under global warming, different Shared Socioeconomic Pathway (SSP) scenarios within CMIP6 simulations could replicate these relevant historical fatigue increments up to 2100 in energetic locations of the oceans that can drastically affect the decisions of stakeholders and government marine planning (Moverley Smith et al., 2022). To develop a screening on various future sea conditions which are sensitive for the mechanical system using their probability occurrences can also give a simple qualitative approach to this problem of long-term fatigue evolution.

CRediT authorship contribution statement

Alain Ulazia: Writing – original draft, Visualization, Validation, Supervision, Project administration, Methodology, Formal analysis, Data curation, Conceptualization. **Hodei Ezpeleta:** Writing – review & editing, Writing – original draft, Visualization, Methodology, Investigation, Data curation, Conceptualization. **Gabriel Ibarra-Berastegi:** Writing – review & editing, Writing – original draft, Supervision, Software, Formal analysis, Data curation, Conceptualization. **Jon Sáenz:** Writing – review & editing, Writing – original draft, Visualization, Validation, Supervision, Software, Resources, Data curation, Conceptualization. **Nahia Martinez-Iturricastillo:** Writing – review & editing, Writing – original draft, Visualization, Validation, Supervision, Formal analysis, Data curation, Conceptualization. **John V. Ringwood:** Writing – review & editing, Writing – original draft, Software, Resources, Methodology, Conceptualization.

Declaration of competing interest

The authors declare that they have no known competing financial interests or personal relationships that could have appeared to influence the work reported in this paper.

Data availability

Data will be made available on request.

Acknowledgements

This study is part of project PID2020-116153RB-I00 funded by Ministerio de Ciencia e Innovación, Spain MCIN/AEI/10.13039/501100011033 and received funding from the University of Basque Country, Spain (UPV/EHU project GIU20/008).

References

Allen, C., Viscelli, A., Dagher, H., Goupee, A., Gaertner, E., Abbas, N., Hall, M., Barter, G., 2020. Definition of the Umaine Volturnus-S Reference Platform Developed for the IEA Wind 15-Megawatt Offshore Reference Wind Turbine. Tech. Rep., National Renewable Energy Lab.(NREL), Golden, CO (United States).

Babarit, A., Gilloteaux, J.-C., Clodic, G., Duchet, M., Simoneau, A., Platzer, M.F., 2018. Techno-economic feasibility of fleets of far offshore hydrogen-producing wind energy converters. Int. J. Hydrogen Energy 43 (15), 7266–7289.

Block, P., Souza Filho, F., Sun, L., Kwon, H.-H., 2009. A streamflow forecasting framework using multiple climate and hydrological models. J. Am. Water Resour. Assoc. 45 (4), 828–843. http://dx.doi.org/10.1111/j.1752-1688.2009.00327.x.

Bloomfield, H., Shaffrey, L., Hodges, K., Vidale, P., 2018. A critical assessment of the long-term changes in the wintertime surface arctic oscillation and northern hemisphere storminess in the ERA20C reanalysis. Environ. Res. Lett. 13 (9), 094004.

Carreno-Madinabeitia, S., Ibarra-Berastegi, G., Sáenz, J., Ulazia, A., 2021. Long-term changes in offshore wind power density and wind turbine capacity factor in the Iberian Peninsula (1900–2010). Energy 226, 120364.

Carreno-Madinabeitia, S., Serras, P., Ibarra-Berastegui, G., Sáenz, J., Ulazia, A., 2024. Future electricity production at mutriku wave energy plant estimated from CMIP6 wave climate projections (2015–2100). Ocean Eng. 291, 116624.

Chen, J., 2011. Development of offshore wind power in China. Renew. Sustain. Energy Rev. 15 (9), 5013–5020.

Copernicus C3S, 2021. Changing the reference period from 1981–2020 to 1991–2020 for the C3s climate bulletin. URL https://climate.copernicus.eu/sites/default/files/2021-02/C3S_Climate_Bulletin_change_from_1981-2010_to_1991-2020_reference_period_v08-Feb-20_all.pdf.

Du, J., Wang, H., Wang, S., Song, X., Wang, J., Chang, A., 2020. Fatigue damage assessment of mooring lines under the effect of wave climate change and marine corrosion. Ocean Eng. 206, 107303.

EirGrid Group, 2023. Renewable Electricity Support Scheme, ORESS 1 Provisional. Tech. Rep., EirGrid, URL https://www.eirgridgroup.com/site-files/library/EirGrid/ORESS-1-Provisional-Auction-Results-2023-(OR1PAR).pdf. Accessed: July 31, 2023.

Eyring, V., Bony, S., Meehl, G.A., Senior, C.A., Stevens, B., Stouffer, R.J., 2016. Overview of the coupled model intercomparison project phase 6 (CMIP6) experimental design and organization. Geosci. Model Dev. 9 (1), 1931–1958.

Freeman, E., Kent, E.C., Brohan, P., Cram, T., Gates, L., Huang, B., Liu, C., Smith, S.R., Worley, S.J., Zhang, H.-M., 2019. The international comprehensive ocean-atmosphere data set–meeting users needs and future priorities. Front. Mar. Sci. 6, 435.

Fusco, F., Nolan, G., Ringwood, J.V., 2010. Variability reduction through optimal combination of wind/wave resources–an Irish case study. Energy 35 (1), 314–325.

Gaertner, E., Rinker, J., Sethuraman, L., Zahle, F., Anderson, B., Barter, G.E., Abbas, N.J., Meng, F., Bortolotti, P., Skrzypinski, W., et al., 2020. IEA Wind TCP Task 37: Definition of the IEA 15-Megawatt Offshore Reference Wind Turbine. Tech. Rep., National Renewable Energy Lab.(NREL), Golden, CO (United States).

Gallagher, S., Tiron, R., Whelan, E., Gleeson, E., Dias, F., Dias, F., McGrath, R., 2016. The nearshore wind and wave energy potential of Ireland: A high resolution assessment of availability and accessibility. Renew. Energy 88, 494–516. http://dx.doi.org/10.1016/J.RENENE.2015.11.010.

Gaughan, E., Fitzgerald, B., 2020. An assessment of the potential for co-located offshore wind and wave farms in Ireland. Energy 200, 117526. http://dx.doi.org/10.1016/J.ENERGY.2020.117526.

Ghil, D.S., Allen, M.R., 2002. Climate Patterns: Past, Present and Future. Cambridge University Press, Cambridge, UK.

Golparvar, B., Papadopoulos, P., Ezzat, A.A., Wang, R.-Q., 2021. A surrogate-model-based approach for estimating the first and second-order moments of offshore wind power. Appl. Energy 299, 117286.

Goncalves, J., Rosa, M., Guedes Soares, C., 2017. Suction anchors for floating offshore wind turbines. Renew. Energy 105, 90–103. http://dx.doi.org/10.1016/j.renene.2016.11.062.

Government of Ireland, 2023. Policy statement on the framework for phase two offshore wind. URL https://www.gov.ie/en/publication/f3bb6-policy-statement-on-the-framework-for-phase-two-offshore-wind/. Accessed: July 31, 2023.

Guo, Y., Wang, H., Lian, J., 2022. Review of integrated installation technologies for offshore wind turbines: Current progress and future development trends. Energy Convers. Manage. 255, 115319.

Haid, L., Stewart, G., Jonkman, J., Robertson, A., Lackner, M., Matha, D., 2013. Simulation-length requirements in the loads analysis of offshore floating wind turbines. In: International Conference on Offshore Mechanics and Arctic Engineering. Vol. 55423, American Society of Mechanical Engineers, V008T09A091.

Hayes, L., Stocks, M., Blakers, A., 2021. Accurate long-term power generation model for offshore wind farms in europe using ERA5 reanalysis. Energy 229, 120603.

Hayman, G., Buhl, Jr., M., 2012. Mlife Users Guide for Version 1.00. Vol. 74, National Renewable Energy Laboratory, Golden, CO, p. 112, (75).

Hersbach, H., Bell, B., Berrisford, P., Hirahara, S., Horányi, A., Muñoz-Sabater, J., Nicolas, J., Peubey, C., Radu, R., Schepers, D., et al., 2020. The ERA5 global reanalysis. Q. J. R. Meteorol. Soc. 146 (730), 1999–2049.

Higgins, P., Foley, A., 2014. The evolution of offshore wind power in the United Kingdom. Renew. Sustain. Energy Rev. 37, 599–612.

Holthuijsen, L.H., 2010. Waves in oceanic and coastal waters. Editorial.

Hsu, S., 2003. Estimating overwater friction velocity and exponent of power-law wind profile from gust factor during storms. J. Waterw. Port Coast. Ocean Eng. 129 (4), 174–177.

Hübler, C., Rolfes, R., 2021. Analysis of the influence of climate change on the fatigue lifetime of offshore wind turbines using imprecise probabilities. Wind Energy 24 (3), 275–289.

Ibarra-Berastegi, G., Ulazia, A., Sáenz, J., Serras, P., Rojí, S.J.G., Esnaola, G., Iglesias, G., 2021. The power flow and the wave energy flux at an operational wave farm: Findings from Mutriku, Bay of Biscay. Ocean Eng. 227, 108654.

Ibarra-Berastegui, G., Sáenz, J., Ulazia, A., Sáenz-Aguirre, A., Esnaola, G., 2023. CMIP6 projections for global offshore wind and wave energy production (2015–2100). Sci. Rep. 13 (1), 18046.

James, M., Haldar, S., Varghese, R., Bhattacharya, S., Pakrashi, V., 2023. Climate change effects on offshore wind turbines. In: Wind Energy Engineering. Elsevier, pp. 413–422.

Jang, D., Kim, K., Kim, K.-H., Kang, S., 2022. Techno-economic analysis and Monte Carlo simulation for green hydrogen production using offshore wind power plant. Energy Convers. Manage. 263, 115695.

Jenniches, S., Worrell, E., Fumagalli, E., 2019. Regional economic and environmental impacts of wind power developments: A case study of a German region. Energy Policy 132, 499–514.

Jin, S., Zheng, S., Greaves, D., 2022. On the scalability of wave energy converters. Ocean Eng. 243, 110212.

Jonkman, J., 2010. Definition of the Floating System for Phase IV of OC3. Tech. Rep., National Renewable Energy Lab.(NREL), Golden, CO (United States).

Jonkman, J.M., Branlard, E.S., Jasa, J.P., 2021. Influence of wind turbine design parameters on linearized physics-based models in OpenFAST. Wind Energy Sci. Discuss. 2021, 1–27.

Jonkman, J., Butterfield, S., Musial, W., Scott, G., 2009. Definition of a 5-MW Reference Wind Turbine for Offshore System Development. Tech. Rep., National Renewable Energy Lab.(NREL), Golden, CO (United States).

Jonkman, J., Matha, D., 2010. Quantitative Comparison of the Responses of Three Floating Platforms. Tech. Rep., National Renewable Energy Lab.(NREL), Golden, CO (United States).

Kalogeri, K., Kalogirou, S.A., Karagiannis, G., Papadopoulos, A., Hatzichristos, T.G., 2021. Progress of combined wind and wave energy harvesting devices and related coupling simulation techniques. Energy J. 42 (2), 347–376. http://dx.doi.org/10.5547/ISSN0195-6574.42.2.347.

Kalvig, S.M., Manger, E., Hjertager, B.H., Jakobsen, J.B., 2014. Wave influenced wind and the effect on offshore wind turbine performance. Energy Procedia 53, 202–213. http://dx.doi.org/10.1016/J.EGYPRO.2014.07.229.

Kardakaris, K., Boufidi, I., Soukissian, T., 2021. Offshore wind and wave energy complementarity in the greek seas based on ERA5 data. Atmosphere 12 (10), 1360.

Lackner, M.A., 2009. Controlling platform motions and reducing blade loads for floating wind turbines. Wind Eng. 33 (6), 541–553.

Li, X., Gao, H., 2015. Load mitigation for a floating wind turbine via generalized H_∞ structural control. IEEE Trans. Ind. Electron. 63 (1), 332–342.

Li, B., Shi, H., Rong, K., Geng, W., Wu, Y., 2023. Fatigue life analysis of offshore wind turbine under the combined wind and wave loadings considering full-directional wind inflow. Ocean Eng. 281, 114719. http://dx.doi.org/10.1016/j.oceaneng.2023.114719, URL https://www.sciencedirect.com/science/article/pii/S0029801823011034.

Liang, Y., Wu, C., Zhang, M., Ji, X., Shen, Y., He, J., Zhang, Z., 2022. Statistical modelling of the joint probability density function of air density and wind speed for wind resource assessment: A case study from China. Energy Convers. Manage. 268, 116054.

Manwell, J.F., McGowan, J.G., Rogers, A.L., 2010. Wind Energy Explained: Theory, Design and Application. John Wiley & Sons.

Maraun, D., 2010. Bias correction of daily precipitation simulated by a regional climate model: a comparison of methods. Int. J. Climatol. 30 (4), 611–623. http://dx.doi.org/10.1002/joc.1936.

Maritime Area, 2023. Maritime area regulatory authority. https://www.maritimeregulator.ie/. Accessed: July 31, 2023.

Morim, J., Hemer, M., Wang, X.L., Cartwright, N., Trenham, C., Semedo, A., Young, I., Bricheno, L., Camus, P., Casas-Prat, M., et al., 2019. Robustness and uncertainties in global multivariate wind-wave climate projections. Nature Clim. Change 9 (9), 711–718.

Moverley Smith, B., Clayton, R., van der Weijde, A.H., Thies, P.R., 2022. Evaluating technical and financial factors for commercialising floating offshore wind: A stakeholder analysis. Wind Energy 25 (11), 1959–1972.

Murtagh, F., Legendre, P., 2014. Ward's hierarchical agglomerative clustering method: which algorithms implement ward's criterion? J. Classification 31, 274–295.

Natarajan, A., Hansen, M.H., Wang, S., 2016. Design load basis for offshore wind turbines: DTU wind energy report no. E-0133.

Nguyen, T.T., Du, Y., Chen, D., Wang, X., Chen, X., Qiao, F., Hu, J., 2021. Future changes in wind and wave climates over the global ocean in CMIP6. Clim. Dynam. 56 (5–6), 1631–1652.

Omrani, N., Aumont, O., Dufour, A., Dussin, R., Hamdi, L., Meyssignac, B., Moine, M.-P., Mouysset, L., Planton, S., Rousset, C., et al., 2020. Assessment of CMIP6 wave and wind climate projections over the global ocean. Clim. Dynam. 55 (5–6), 1631–1652.

OpenFAST v3.1.0 available at https://github.com/OpenFAST/openfast. (accessed on 14 May 2023).

Penalba, M., Ulazia, A., Ibarra-Berastegui, G., Ringwood, J., Sáenz, J., 2018. Wave energy resource variation off the west coast of Ireland and its impact on realistic wave energy converters' power absorption. Appl. Energy 224, 205–219.

Penalba, M., Ulazia, A., Saénz, J., Ringwood, J.V., 2020. Impact of long-term resource variations on wave energy farms: The Icelandic case. Energy 192, 116609.

Pereira, E.B., Martins, F.R., Pes, M.P., da Cruz Segundo, E.I., Lyra, A.d.A., 2013. The impacts of global climate changes on the wind power density in Brazil. Renew. Energy 49, 107–110.

Piani, C., Haerter, J.O., Coppola, E., 2010. Statistical bias correction for daily precipitation in regional climate models over europe. Theor. Appl. Climatol. 99 (1), 187–192. http://dx.doi.org/10.1007/s00704-009-0134-9.

Poli, P., Hersbach, H., Dee, D.P., Berrisford, P., Simmons, A.J., Vitart, F., Laloyaux, P., Tan, D.G., Peubey, C., Thépaut, J.-N., et al., 2016. ERA-20C: An atmospheric reanalysis of the twentieth century. J. Clim. 29 (11), 4083–4097.

Quarton, D., et al., 2005. An International Design Standard for Offshore Wind Turbines: IEC 61400-3. Garrad Hassan and Partners, Ltd, Bristol, UK.

Remmers, T., Cawkwell, F., Desmond, C.J., Murphy, J., Politi, E., 2019. The potential of advanced scatterometer (ASCAT) 12.5 km coastal observations for offshore wind farm site selection in Irish waters. Energies 12 (2), 206. http://dx.doi.org/10.3390/EN12020206.

Rojas, R., Feyen, L., Dosio, A., Bavera, D., 2011. Improving pan-European hydrological simulation of extreme events through statistical bias correction of RCM-driven climate simulations. Hydrol. Earth Syst. Sci. 15 (8), 2599–2620. http://dx.doi.org/10.5194/hess-15-2599-2011.

Saenz-Aguirre, A., Ulazia, A., Ibarra-Berastegi, G., Saenz, J., 2022. Floating wind turbine energy and fatigue loads estimation according to climate period scaled wind and waves. Energy Convers. Manage. 271, 116303.

Shafiee, M., 2023. Failure analysis of spar buoy floating offshore wind turbine systems. Innov. Infrastruct. Solut. 8 (1), 28.

Sun, F., Roderick, M.L., Lim, W.H., Farquhar, G.D., 2011. Hydroclimatic projections for the murray-darling basin based on an ensemble derived from intergovernmental panel on climate change AR4 climate models. Water Resour. Res. 47 (12), http://dx.doi.org/10.1029/2010WR009829.

Tao, T., Long, K., Yang, T., Liu, S., Yang, Y., Guo, X., Chen, M., 2023. Quantitative assessment on fatigue damage induced by wake effect and yaw misalignment for floating offshore wind turbines. Ocean Eng. 288, 116004. http://dx.doi.org/10.1016/j.oceaneng.2023.116004, URL https://www.sciencedirect.com/science/article/pii/S0029801823023880.

Teutschbein, C., Seibert, P., 2011. Intercomparison of bias-correction methods for monthly temperature and precipitation simulated by multiple climate models. Clim. Dynam. 37 (1), 33–51. http://dx.doi.org/10.1007/s00382-010-0758-3.

The MathWorks Inc., 2022. MATLAB version: 9.13.0 (r2022b). URL https://www.mathworks.com.

Ulazia, A., Penalba, M., Ibarra-Berastegui, G., Ringwood, J., Sáenz, J., 2019a. Reduction of the capture width of wave energy converters due to long-term seasonal wave energy trends. Renew. Sustain. Energy Rev. 113, 109267.

Ulazia, A., Penalba, M., Rabanal, A., Ibarra-Berastegi, G., Ringwood, J., Sáenz, J., 2018. Historical evolution of the wave resource and energy production off the chilean coast over the 20th century. Energies 11 (9), 2289.

Ulazia, A., Sáenz, J., Ibarra-Berastegi, G., González-Rojí, S.J., Carreno-Madinabeitia, S., 2019b. Global estimations of wind energy potential considering seasonal air density changes. Energy 187, 115938.

Ulazia, A., Saenz, J., Ibarra-Berastegui, G., 2016. Sensitivity to the use of 3DVAR data assimilation in a mesoscale model for estimating offshore wind energy potential. a case study of the iberian northern coastline. Appl. Energy 180, 617–627.

Ulazia, A., Sáenz, J., Ibarra-Berastegui, G., González-Rojí, S.J., Carreno-Madinabeitia, S., 2017. Using 3DVAR data assimilation to measure offshore wind energy potential at different turbine heights in the west mediterranean. Appl. Energy 208, 1232–1245.

Ulazia, A., Sáenz, J., Saenz-Aguirre, A., Ibarra-Berastegui, G., Carreno-Madinabeitia, S., 2023a. Paradigmatic case of long-term colocated wind–wave energy index trend in canary islands. Energy Convers. Manage. 283, 116890.

Ulazia, A., Saenz-Aguirre, A., Ibarra-Berastegui, G., Sáenz, J., Carreno-Madinabeitia, S., Esnaola, G., 2023b. Performance variations of wave energy converters due to global long-term wave period change (1900–2010). Energy 268, 126632.

Vamsikrishna, R., Rao, D.N., Devara, P., 2012. Bias correction of regional climate model simulations for hydrological climate-change impact studies: Review and evaluation of different methods. J. Hydrol. 414–415, 204–221. http://dx.doi.org/10.1016/j.jhydrol.2011.11.011.

2023. Warning of a forthcoming collapse of the Atlantic meridional overturning circulation. 14 (1), 4254. http://dx.doi.org/10.1038/s41467-023-39810-w. URL https://www.nature.com/articles/s41467-023-39810-w.

Wilkie, D., Galasso, C., 2020. Impact of climate-change scenarios on offshore wind turbine structural performance. Renew. Sustain. Energy Rev. 134, 110323.

2017. WMO Guidelines on the Calculation of Climate Normals. Tech. Rep. WMO-No. 1203, World Meteorological Organization, Geneva, Switzerland, p. 18.

Wohland, J., Omrani, N.E., Keenlyside, N., Witthaut, D., 2019. Significant multidecadal variability in German wind energy generation. Wind Energy Sci. 4 (3), 515–526.